C-terminal HSP90 inhibitor NCT-58 impairs the cancer stem-like phenotype and enhances chemotherapy efficacy in TNBC

EUNSUN JUNG[1-3*], YOON-JAE KIM[1,3*], KYOUNGMIN LEE[1,3*], SEOJIN JANG[1,2*], SOEUN PARK[1,2], EUNHYE OH[1,2], MINSU PARK[1,2], SEONGJAE KIM[1,2], DONGMI KO[1,2], YONG KOO KANG[1,3], KEE DAL NAM[1,3], LEE FARRAND[4], CONG-TRUONG NGUYEN[5], MINH THANH LA[5], JIHYAE ANN[5], JEEWOO LEE[5], JI YOUNG KIM[1,3] and JAE HONG SEO[1-3]

[1]Division of Medical Oncology, Department of Internal Medicine, Korea University College of Medicine, Korea University, Seoul 152-703, Republic of Korea; [2]Brain Korea 21 Program for Biomedical Science, Korea University College of Medicine, Korea University, Seoul 152-703, Republic of Korea; [3]Department of Biomedical Research Center, Korea University Guro Hospital, Korea University, Seoul 08308, Republic of Korea; [4]Adelaide Medical School, Faculty of Health and Medical Sciences, The University of Adelaide, Adelaide, South Australia 5000, Australia; [5]Laboratory of Medicinal Chemistry, College of Pharmacy, Seoul National University, Seoul 08826, Republic of Korea

Received July 14, 2025; Accepted October 27, 2025

DOI: 10.3892/or.2025.9018

Abstract. Treatment options for triple-negative breast cancer (TNBC) are limited because they typically harbor a high cancer stem-like population and exhibit a relatively aggressive metastatic phenotype. Heat shock protein 90 (HSP90), a molecular chaperone that regulates diverse oncogenic client proteins, has emerged as a compelling therapeutic target owing to its involvement in key tumor-promoting processes, such as uncontrolled proliferation, angiogenesis and metastasis. Owing to the undesirable induction of a compensatory heat shock response (HSR) and systemic toxicity, classical N-terminal inhibitors of HSP90 have failed in clinical trials. The impact of a rationally designed novel inhibitor of the HSP90 C-terminus in TNBC cells was investigated. NCT-58 eliminates rapidly proliferating tumor cells accompanied by simultaneous degradation of AKT, MEK and STAT3, and effectively eradicates the cancer stem-like population (breast cancer stem cells) in both human MDA-MB-231 and murine 4T1 cells. The latter phenomenon is accompanied by reductions in the activity of ALDH1 and the $CD44^{high}/CD24^{low}$ stem-like population, as well as impairment of mammosphere formation. Furthermore, NCT-58 markedly impairs cell migration, coinciding with the collapse of HSP90 client cytoskeletal proteins, including vimentin and F-actin, in MDA-MB-231 cells *in vitro*. A synergistic effect was observed when NCT-58 was combined with paclitaxel or doxorubicin in MDA-MB-231 cells. Collectively, these findings indicated that targeting the C-terminal domain of HSP90 with NCT-58 is a promising therapeutic strategy for the treatment of molecularly heterogeneous TNBC.

Correspondence to: Professor Jae Hong Seo or Dr Ji Young Kim, Department of Biomedical Research Center, Korea University Guro Hospital, Korea University, 148 Gurodong, Guro, Seoul 08308, Republic of Korea
E-mail: cancer@korea.ac.kr
E-mail: amaryllis1210@gmail.com

*Contributed equally

Key words: HSP90 inhibitor, NCT-58, triple-negative breast cancer, cancer stem cells, heat shock response

Introduction

Triple-negative breast cancer (TNBC) is the most aggressive subtype of breast cancer, defined by the lack of estrogen receptor (ER), progesterone receptor (PR), and human epidermal growth factor receptor 2 (HER2) expression in tumor cells. It is characterized by a more aggressive growth pattern and more enhanced metastatic potential than other subtypes. Despite advancements in breast cancer therapeutics that have contributed to improved mortality rates, patients with TNBC continue to face substantial clinical challenges as they are generally ineligible for existing targeted therapies (1).

HSP90 is frequently upregulated in cancer, with expression levels reported to be 2- to 10-fold higher than those in normal tissues (2). In breast cancer, its overexpression correlates with adverse clinicopathological features, including larger tumor size, higher nuclear grade, and poor prognosis, particularly in early stage disease (3). Functionally, HSP90 acts as a molecular chaperone that supports the folding and stability of more than 200 target proteins involved in oncogenic processes such as cellular proliferation, resistance to apoptosis, angiogenesis and metastatic progression (4). HSP90 drives tumor progression and therapy resistance by sustaining pro-survival signaling pathways, such as JAK/STAT3, AKT and MEK (5,6). Given its central role in

sustaining oncogenic signaling, HSP90 has emerged as a compelling therapeutic target for TNBC. Therefore, pharmacological inhibition of HSP90 offers a promising strategy for simultaneously disrupting multiple oncogenic pathways in this aggressive breast cancer subtype (7).

Emerging evidence has emphasized the key role of cancer stem cells (CSCs) in tumor initiation, invasion and metastasis, particularly in TNBC, where they drive chemoresistance and metastasis, leading to treatment failure (8). Previous studies have reported that HSP90 and its co-chaperones are highly implicated in the maintenance of the CSC phenotype, expression of EMT-related genes, and stability of pluripotent transcription factors such as Nanog and Oct4 (9-12). Targeting HSP90 not only disrupts pro-survival signaling pathways but also impairs the maintenance of the CSC phenotype, thereby reducing chemoresistance and metastatic potential, and highlighting its dual role as a promising therapeutic target in TNBC management.

HSP90 comprises three domains: A N-terminal domain (NTD) containing an ATP-binding pocket, a middle domain (MD), and a C-terminal domain (CTD) required for dimerization (13). Most HSP90 inhibitors in clinical trials target the N-terminus, but none have received FDA approval owing to serious issues arising from the induction of the heat shock response (HSR), off-target effects, and organ toxicity (14,15). NCT-58, a C-terminal HSP90 inhibitor that interferes with the binding of ATP to its CTD, was developed. NCT-58 is one of 90 synthesized O-substituted analogs of the B- and C-ring-truncated scaffolds of deguelin, a naturally occurring rotenoid. It was observed that NCT-58 exerted antitumor activity in HER2-positive breast cancer cells by downregulating HER2 and inducing apoptosis (16). In the present study, the mechanism underlying the novel effects of NCT-58 on apoptosis, breast cancer stem cells (BCSC)-like properties, and cell migration in TNBC cells, was explored. Furthermore, the potential of NCT-58 combined with paclitaxel or doxorubicin was evaluated, and its potential as a multifaceted therapeutic strategy for TNBC was highlighted.

Materials and methods

Reagents and antibodies. NCT-58 was synthesized according to a previously established protocol (17). For all experiments, NCT-58 was prepared as a stock solution (10 mM) in dimethyl sulfoxide (DMSO) and vehicle controls contained the corresponding final concentration of DMSO (0.1% v/v). Chemicals, including propidium iodide (PI), DMSO and Triton X-100, were purchased from MilliporeSigma. Protease and phosphatase inhibitor tablets were obtained from Roche Applied Science. The primary antibodies used for western blotting and immunocytochemistry were specific to vimentin, STAT3, phospho-STAT3 (Tyr705), AKT, phospho-AKT (Ser473), MEK, phospho-MEK (Ser218/222), PARP, cleaved PARP, cleaved caspase-3, and -7, heat shock transcription factor-1 (HSF)-1, HSP70, cyclin D1, survivin, F-actin (Texas Red™-X Phalloidin) and GAPDH. Secondary antibodies included horseradish peroxidase (HRP)-conjugated anti-mouse and anti-rabbit IgG and Alexa Fluor 488/594-labeled anti-mouse and anti-rabbit IgG.

Cell culture. The TNBC cell lines MDA-MB-231 (PerkinElmer, Inc.), Hs578T (American Type Culture Collection; ATCC), BT549 and 4T1 (Japanese Collection of Research Bioresources Cell Bank), and the cell line 293 (Korean Cell line Bank) were maintained in MEM or RPMI-1640 supplemented with 10% FBS and 100 U/ml penicillin-streptomycin (Gibco; Thermo Fisher Scientific, Inc.). The normal human mammary epithelial cell line MCF10A (ATCC) was cultured in Mammary Epithelial Cell Growth Basal Medium, including hEGF (20 ng/ml), insulin (10 μg/ml), hydrocortisone (0.5 μg/ml) and bovine pituitary extract (50 μg/ml) (SingleQuots™ Kit; Lonza Group, Ltd.) containing streptomycin-penicillin (100 U/ml). The cells were then incubated at 37˚C in an atmosphere containing 5% CO_2.

Cell viability assay. Cell viability was measured using the CellTiter 96® Aqueous One Solution Cell Proliferation Assay [MTS, 3-(4, 5-dimethylthiazol-2-yl)-5-(3-carboxymethoxyphenyl)-2-(4-sulfophenyl)-2H-tetrazolium] (Promega Corporation) according to the manufacturer's instructions. The MTS reagent, which is soluble in cell culture medium, was added directly to the cells. The quantity of purple formazan product was determined by measuring the absorbance at 490 nm using a microplate reader (Agilent BioTek 800 TS; Agilent Technologies, Inc.). Percentage cell viability was calculated relative to that of the untreated control (set at 100%). IC_{50} values were determined by fitting sigmoidal dose-response curves using nonlinear regression analysis in GraphPad Prism 9.0 (Dotmatics).

Cell cycle and Sub-G1 analysis. Cell cycle distribution and sub-G1 populations were analyzed using flow cytometry. Cells were harvested at 70-80% confluence, washed twice with cold phosphate-buffered saline (PBS), and fixed by dropwise addition of pre-chilled 95% ethanol containing 0.5% Tween-20. The samples were then incubated at -20˚C overnight to ensure complete fixation. Following fixation, cells were centrifuged (7,160 x g), resuspended in staining buffer containing propidium iodide (50 μg/ml) and RNase A (50 μg/ml), and incubated for 30 min at room temperature in the dark. DNA content was assessed using a Beckman Coulter Expo flow cytometer (Beckman Coulter, Inc.) and data were analyzed using FlowJo software v10.10 (BD Biosciences).

Aldefluor-positive assay, $CD44^{high}/CD24^{low}$ staining. To evaluate ALDH1 enzymatic activity, cells were treated using the Aldefluor™ assay kit (Stemcell Technologies, Inc.) in accordance with the supplier's protocol. Briefly, cells ($0.5x10^6$) were suspended in assay buffer containing 1 μM BODIPY-amino-acet-aldehyde and incubated at 37˚C for 45 min. Diethyl-amino-benzaldehyde (50 mM) was added to the control sample to inhibit ALDH1 activity and establish gating parameters for the Aldefluor-positive population during flow cytometric analysis. To identify stem-like cell populations exhibiting the $CD44^{high}/CD24^{low}$ phenotype, cells were incubated at 4˚C for 30 min with FITC-labeled anti-CD24 and PE-labeled anti-CD44 antibodies (1:50; BD Biosciences). FITC- and PE-conjugated isotype-matched mouse IgG antibodies were used as controls for non-specific staining. The labeled cells were subsequently subjected to flow cytometry.

Mammosphere formation assay. To assess sphere-forming capacity, 4T1 cells were seeded at a density of $3x10^5$ cells/ml in ultralow attachment plates (Corning, Inc.) and cultured in HuMEC basal serum-free medium (Gibco; Thermo Fisher Scientific, Inc.), supplemented with B27 (1:50; Invitrogen; Thermo Fisher Scientific, Inc.), 20 ng/ml basic fibroblast growth factor (bFGF; MilliporeSigma), 20 ng/ml mouse epidermal growth factor (EGF, MilliporeSigma), 4 μg/ml heparin, 1% antibiotic-antimycotic solution, and 15 μg/ml gentamycin. The number and volume of mammospheres were determined using an Olympus CKX53 inverted microscope, and the sphere size was quantified using ImageJ software (v1.54; National Institutes of Health). Mammosphere volumes were calculated using the formula: Volume=$4/3x3.14xr^3$.

C-terminal HSP90 inhibition assay. A C-terminal HSP90α Inhibitor Screening Kit (BPS Bioscience) was used to evaluate inhibition of the interaction between the C-terminal region of HSP90α and its co-chaperone peptidylprolyl isomerase D (PPID) by HSP90 inhibitors, as previously described (11,18). The assay was conducted in 384-well Optiplates (PerkinElmer, Inc.) and luminescence signals were detected using the AlphaScreen® technology on a Varioskan LUX™ microplate reader (Thermo Fisher Scientific, Inc.).

N-terminal HSP90 binding activity assay. To assess compound binding affinity to the NTD of HSP90α, a fluorescence-based competitive binding assay (HSP90α N-terminal Assay Kit; BPS Bioscience) was conducted in accordance with the manufacturer's guidelines. Test compounds (ranging from 0-1,000 nM in DMSO) were mixed with a reaction solution comprising FITC-tagged geldanamycin (100 nM) and recombinant HSP90α protein (17 ng/μl), followed by incubation at room temperature for 3 h. Fluorescence intensity was then measured at an excitation wavelength of 485 nm and emission at 530 nm using a SpectraMax Gemini EM microplate reader (Molecular Devices, LLC) to assess the binding activity to the NTD of HSP90.

Wound healing assay. Cells were plated in 96-well ImageLock plates (Essen Bioscience) and grown until they reached ~90% confluency. A uniform wound was created using a 96-pin WoundMaker, followed by washing with PBS to eliminate detached cells. Immediately after scratch formation, cells were exposed to varying concentrations of NCT-58. Cell migration was monitored in real time by capturing images hourly for 25 to 50 h using an IncuCyte ZOOM Live-Cell Imaging System (Essen Bioscience). The progression of wound closure was quantified using the IncuCyte™ Scratch Wound Cell Migration analysis software (Essen BioScience).

Immunoblot analysis. Membranes were incubated overnight at 4˚C with primary antibodies diluted in 5% bovine serum albumin (BSA) (Thermo Fisher Scientific, Inc.), targeting the following proteins: AKT (1:2,000), phospho-AKT (1:2,000), MEK (1:2,000), phospho-MEK (1:2,000), STAT3 (1:2,000), phospho-STAT3 (Tyr705, 1:2,000), survivin (1:2,000), cyclin D1 (1:2,000), PARP (1:2,000), cleaved PARP (1:2,000), cleaved caspase-3 (1:1,000), cleaved caspase-7 (1:1,000), and GAPDH (1:3,000). After washing, the membranes were incubated with HRP-conjugated secondary antibodies (anti-rabbit or anti-mouse IgG, 1:3,000-1:5,000). Protein bands were visualized using an enhanced chemiluminescence (ECL) detection system (Thermo Fisher Scientific, Inc.).

Cells were lysed in radioimmunoprecipitation assay buffer (50 mM Tris-HCl, pH 7.5, 150 mM NaCl, 1% NP-40, 0.5% sodium deoxycholate and 0.1% SDS) supplemented with protease and phosphatase inhibitor cocktails (Roche Diagnostics). The lysates were incubated on ice for 30 min and then centrifuged at 25,200 x g for 15 min at 4˚C to remove insoluble debris. The supernatant was collected, and protein concentrations were determined using a BCA assay (Thermo Fisher Scientific, Inc.). Equal amounts of protein (20 μg per lane) were mixed with the sample buffer, boiled for 10 min, separated using 4-15% gradient SDS-PAGE, and transferred onto PVDF membranes (MilliporeSigma). Membranes were blocked with 5% skim milk for 1 h at room temperature and subsequently incubated overnight at 4˚C with primary antibodies diluted in 5% BSA [AKT (1:2,000), phospho-AKT (1:2,000), MEK (1:2,000), phospho-MEK (1:2,000), STAT3 (1:2,000), phospho-STAT3 (Y705; 1:2,000), survivin (1:2,000), cyclin D1 (1:2,000), PARP (1:2,000), cleaved-PARP (1:2,000), cleaved-caspase-3 (1:1,000), cleaved-caspase-7 (1:1,000), and GAPDH (1:3,000)]. The catalog numbers and suppliers of antibodies are included in Table SI. After washing, the membranes were incubated with HRP-conjugated secondary antibodies (1:3,000-1:5,000) for 1 h at room temperature. Protein bands were detected using an Enhanced Chemiluminescence Kit (Thermo Fisher Scientific, Inc.), quantified using AlphaEaseFC software (Alpha Innotech Corporation), and normalized to GAPDH as the internal loading control.

Immunocytochemistry. Cells cultured on 8-well chamber slides (BD Biosciences) were fixed with 4% paraformaldehyde at 4˚C for 2 h, rinsed with PBS, and permeabilized with 0.2% Triton X-100 for 10 min. The cells were then incubated overnight at 4˚C with primary antibodies against HSP70 (1:100), HSF-1 (1:100), vimentin (1:200), or F-actin (1:200) diluted in an antibody diluent (Dako; Agilent Technologies, Inc.). After washing, the cells were treated with fluorescence-conjugated secondary antibodies (Alexa Fluor® 488 or 594). Nuclei were counterstained with DAPI (0.4 μg/ml) and mounted using ProLong™ Gold Antifade Reagent (Thermo Fisher Scientific, Inc.). Fluorescence images were captured using a Carl Zeiss confocal microscope, and the signal intensity was quantified using the intensity profile tool. Immunofluorescence images were acquired under identical sensitivity settings, including exposure time, laser power, and gain, across the control and treated groups. For the nuclear protein HSF1, nuclei were segmented using DAPI staining in ImageJ. The integrated density of HSF1 within each nucleus was normalized to the integrated density of the corresponding DAPI signal (HSF1/DAPI ratio) to correct for nuclear size and DNA content. For cytoplasmic proteins HSP70, corrected total cell fluorescence (CTCF) was calculated as: CTCF=Integrated density-(Area x Background mean intensity) with background values obtained from four cell-free regions per image. Quantification was performed using at least 10 cells from a minimum of three independent fields per condition.

Synergy assessment. To evaluate whether two compounds interact synergistically, additively, or antagonistically, the combination index (CI) was determined using CompuSyn® software (ComboSyn, Inc.; https://www.combosyn.com). A CI value of less than, equal to, or greater than 1 denotes synergism, additive effects, or antagonism, respectively. The fraction affected (Fa) represents the proportion of phenotypic inhibition resulting from treatment with a compound. Fa=percent inhibition of cell viability/100. The Fa-CI plot was generated for each group treated with more than one compound, and the corresponding heat map illustrated the percentage inhibition of cell viability under the combination conditions. The CI values at specific effect levels were then used to construct isobolograms, where data points below, on, or above the line of additivity indicated synergistic, additive, or antagonistic effects, respectively.

Molecular docking analysis. *In silico* molecular docking was conducted using open-access AutoDock Vina-based platforms including DockThor (https://www.dockthor.lncc.br) and CB-Dock2 (https://cadd.labshare.cn/cb-dock2). Upon completion of the docking simulations, both 2D and 3D structures of the protein-ligand complexes were visualized and analyzed using UCSF Chimera 1.16 and BIOVIA Discovery Studio 2021. The predicted binding affinity for the interaction between NCT-58 and the CTD of hHSP90α (PDB ID: 7RY1) was estimated to be-9.5 kcal/mol. The binding site and key interactions were analyzed to identify hydrogen bonds, hydrophobic contacts, and the overall binding pocket conformation.

Statistical analysis. Statistical analyses were performed using the GraphPad Prism 9.0 (GraphPad Software; Dotmatics). Data are presented as the mean ± SEM from at least three independent experiments. Comparisons between groups were conducted using unpaired Student's t-test or one-/two-way ANOVA, as appropriate. For two-way ANOVA, Bonferroni's post-hoc test was used to evaluate multiple comparisons. $P<0.05$ was considered to indicate a statistically significant difference.

Results

NCT-58 exerts an anti-proliferative effect without triggering the HSR. The anti-proliferative effect of NCT-58 in the human TNBC cell lines MDA-MB-231, BT549 and Hs578T, and the murine mammary carcinoma line 4T1, were first evaluated. TNBC cell viability was dose-dependently reduced in the presence of NCT-58 (0-20 μM, 72 h) *in vitro* ($P<0.05$; Figs. 1A and S1; Table SII). The estimated IC_{50} values for NCT-58 were 6.701, 4.685, 7.041 and 2.922 μM in MDA-MB-231, BT549, Hs578T and 4T1, respectively. Based on IC_{50} values, a concentration range of 2-10 μM in MDA-MB-231 and 1-5 μM in 4T1 cells was selected for further experiments including apoptosis, western blot analysis, and cancer stem cell-like characterization. Apoptosis was significantly increased in the presence of NCT-58 at 5 μM in MDA-MB-231 cells and at 2 μM in 4T1 cells ($P<0.05$; Fig. 1B) for 72 h, as evidenced by increased sub-G1 accumulation. Apoptosis induction was confirmed using caspase-3 and caspase-7 activation, concomitant with increased cleavage of PARP, a downstream substrate of caspase-3 ($P<0.01$; Fig. 1C). Further quantitative analysis confirmed an increased ratio of cleaved to total forms of caspase-3, caspase-7 and PARP following NCT-58 treatment ($P<0.05$; Fig. S2A-C).

The C-terminal HSP90 binding activity of NCT-58 was analyzed using the co-chaperone peptidylprolyl isomerase D (PPID), which exhibits high-affinity ligand binding activity to the C-terminus of HSP90. NCT-58 significantly inhibited C-terminal HSP90 activity, as evidenced by the marked inhibition of the specific interaction between PPID and the C-terminus of HSP90 ($P<0.001$; Fig. 1D). Similar results were observed for novobiocin, a potent C-terminal HSP90 inhibitor (19), whereas geldanamycin did not affect this interaction. Furthermore, the competitive HSP90 binding assay with fluorescence-labeled geldanamycin did not show N-terminal HSP90 binding activity of NCT-58 (Fig. 1E). Docking studies using the crystal structure of HSP90 (PDB ID: 7RY1), which includes the middle and CTD, revealed that NCT-58 precisely fits into the dimerization interface of the CTD, which is a critical region required for chaperone function (Fig. 1F). The interaction between NCT-58 and the HSP90 CTD was extensively stabilized by five hydrogen bonds with the key residues Thr495, Gln501, Ser674, Gly675 and Phe676. In addition, a π-anion interaction was observed between NCT-58 and Glu497 of HSP90, further enhancing binding stability (Fig. 1G). These findings highlight how NCT-58 specifically occupies the CTD binding pocket to disrupt dimerization and impair HSP90 function.

Subsequently, it was assessed whether NCT-58 induces the HSR, a limitation of classical N-terminal HSP90 inhibitors. Geldanamycin, the first and most extensively studied N-terminal HSP90 inhibitor, was selected as the reference compound and was used in all experiments requiring an N-terminal HSP90 inhibitor (20,21). The N-terminal HSP90 inhibitor induces the phosphorylation and trimerization of heat shock factor-1 (HSF-1), promoting its nuclear translocation and subsequent upregulation of heat shock proteins (HSPs), such as HSP70 and HSP90, which support pro-survival signaling (15,22). MDA-MB-231 cells were treated with geldanamycin (300 nM), a potent N-terminal HSP90 ATP binding inhibitor, and NCT-58 (300 nM and 10 μM), followed by the assessment of HSF-1 and HSP70 expression. Confocal imaging and intensity analysis revealed no increase in HSF-1 levels upon exposure to NCT-58, whereas geldanamycin considerably increased the accumulation of HSF-1 in the nuclei of MDA-MB-231 cells (Fig. 1H). This finding was further supported by the fact that geldanamycin induced the subsequent upregulation of cytoplasmic HSP70, whereas NCT-58 did not elicit this phenomenon (Fig. 1I).

Accumulating preclinical and clinical evidence has highlighted the significant off-target toxicity of geldanamycin derivatives, which causes undesirable effects in normal tissues (23). Notably, NCT-58 exhibited minimal cytotoxicity at 10 μM in normal mammary gland epithelial MCF10A cells and 293 cells, while geldanamycin caused significant cytotoxicity in both normal cell lines at 100 nM, a 1,000-fold lower concentration ($P<0.001$; Fig. 1J and K).

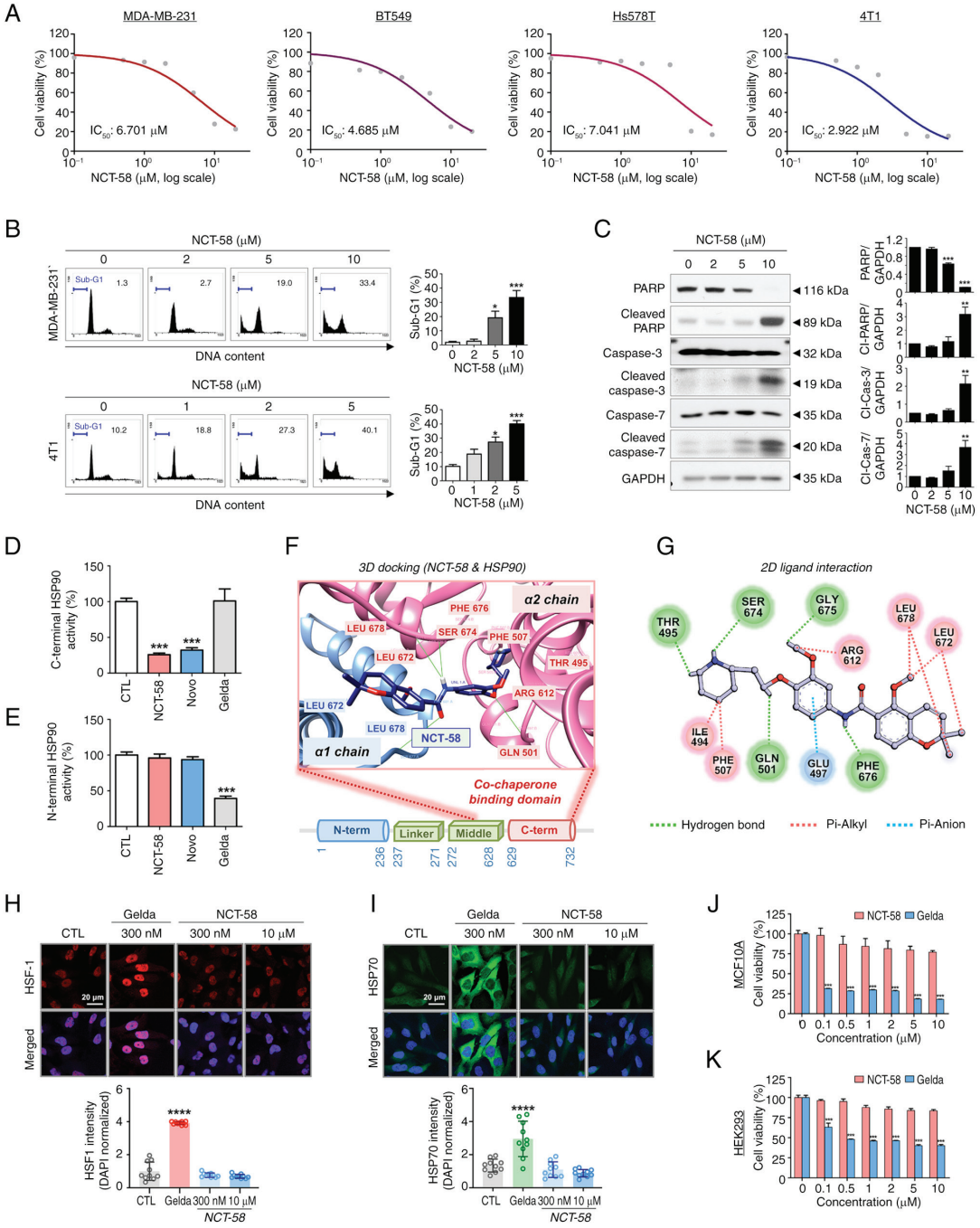

Figure 1. NCT-58 exerts anti-proliferative effect in TNBC cells by targeting the C-terminal domain of HSP90. (A) Four TNBC cell lines, MDA-MB-231, BT549, Hs578T and 4T1 cells were treated with various concentrations of NCT-58 (0-20 μM) for 72 h. Cell viability was assessed using MTS assay, and IC_{50} values were calculated using non-linear regression with a sigmoidal dose-response curve. (B) MDA-MB-231 and 4T1 cells were treated at the indicated concentrations of NCT-58 (0-10 μM) for 72 h. Apoptosis was determined through sub-G1-DNA analysis using flow cytometry. (C) Immunoblot analyses of PARP, cleaved-PARP, caspase-3, cleaved caspase-3, caspase-7 and cleaved caspase-7 protein expression in MDA-MB-231 cells after treatment with NCT-58 (0-10 μM, 72 h). GAPDH was used as an internal loading control. Quantitative graphs of these protein levels. The results are presented as the mean ± SEM of at least three independent experiments and analyzed using one-way ANOVA followed by Bonferroni's post hoc test. (D) Effect of NCT-58 on C-terminal HSP90 binding activity. The inhibitory effect of HSP90 inhibitors (NCT-58, novobiocin or geldanamycin, 500 μM) on the interaction between HSP90α (C-terminal) and its co-chaperone peptidylprolyl isomerase was determined using an HSP90α (C-terminal) inhibitor screening assay. (E) Influence of NCT-58 on N-terminal HSP90 binding activity. The competitive HSP90α binding activity of HSP90 inhibitors (NCT-58, novobiocin or geldanamycin, 1 μM) with FITC-labeled geldanamycin was determined using an HSP90α N-terminal domain assay. (F and G) Molecular docking analysis of NCT-58 binding to the CTD of HSP90 (PDB ID: 7RY1). (F) The binding pose of NCT-58 at the dimerization interface is displayed as a space-filling model. The α1 chain of HSP90 is rendered in a blue ribbon, and the α2 chain in a pink ribbon. Connolly surface representation of the HSP90 CTD, with NCT-58 modeled within the binding interface (docking score=-9.5). (G) A 2D interaction diagram of NCT-58 with key residues in the HSP90 CTD. Hydrogen bonds and π-anion interactions are indicated by dashed green and blue lines, respectively. (H and I) Comparison of the effects of NCT-58 and the N-terminal HSP90 inhibitor geldanamycin on HSF-1 and HSP70 expression. MDA-MB-231 cells were treated with NCT-58 (300 nM and 10 μM) or geldanamycin (300 nM) for 24 h. Cells were immuno-stained for HSF-1 (red, H) or HSP70 (green, I) using DAPI (nuclei, blue). Images were acquired using a confocal microscope, and quantification of immunofluorescence intensity was performed using ImageJ software. Nuclear HSF1 intensity was expressed as the HSF1/DAPI ratio, and cytoplasmic HSP70 intensity was expressed as corrected total cell fluorescence normalized to DAPI. (J and K) Effect of NCT-58 and geldanamycin on cytotoxicity in non-malignant cells. Normal human mammary epithelial MCF10A (J) and 293 (K) cells were treated with various concentrations (0.1-10 μM) of NCT-58 or geldanamycin for 72 h. Cell viability was determined using MTS assay (***P<0.001). *P<0.05, **P<0.01, ***P<0.001 and ****P<0.0001. TNBC, triple-negative breast cancer; Gelda, geldanamycin; Novo, novobiocin; CTD, C-terminal domain.

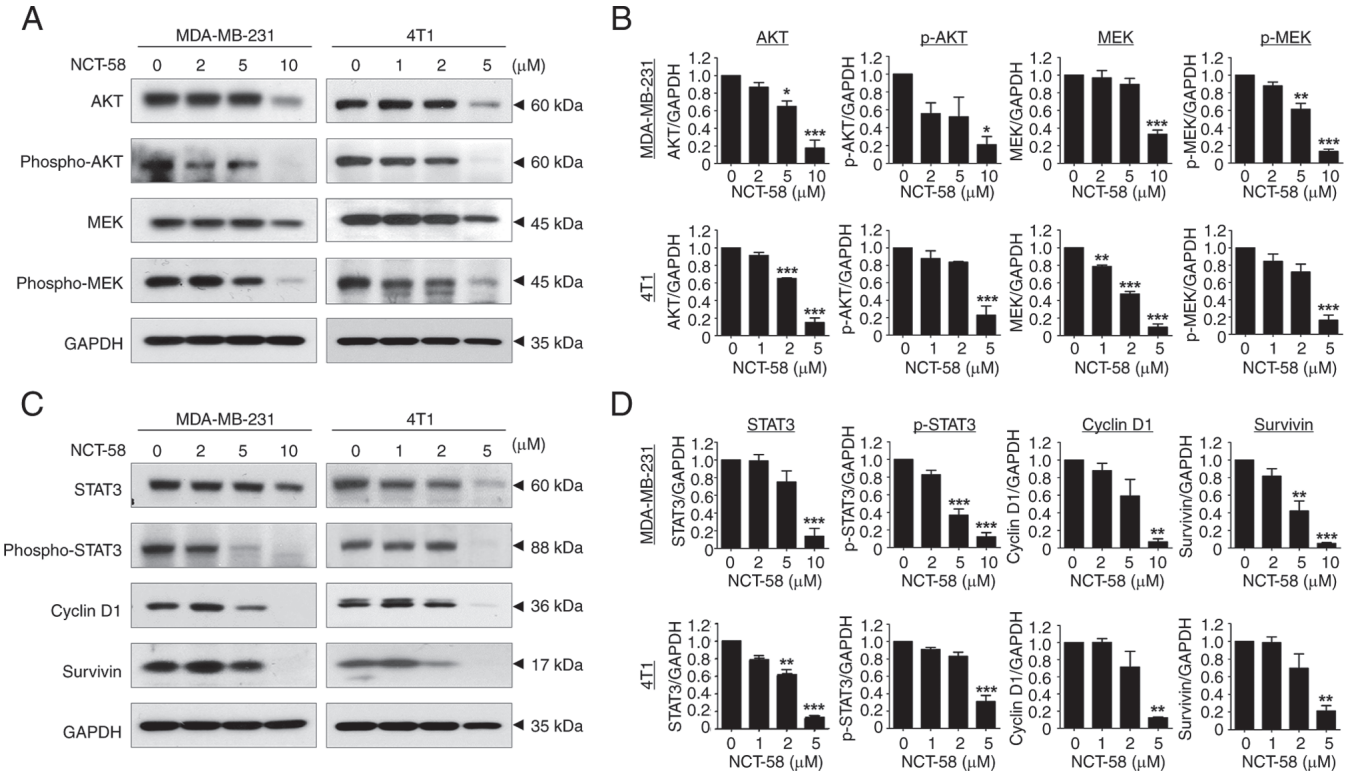

Figure 2. NCT-58 downregulates expression of pro-survival client proteins in triple-negative breast cancer cells. (A) MDA-MB-231 and 4T1 cells were cultured in the presence or absence of NCT-58 (0-10 μM) for 72 h. Expression levels of HSP90 client proteins such as AKT, phospho-AKT (Ser473), MEK and phospho-MEK (Ser218/222) were detected through immunoblotting. GAPDH was used as a loading control. (B) Quantitative graphs represent the ratio of expression of these proteins relative to GAPDH expression after treatment with NCT-58. (C) Immunoblot analyses of STAT3, phospho-STAT3 (Tyr705), protein levels of cyclin D1 and survivin in MDA-MB-231 and 4T1 cells after treatment with NCT-58 (0-10 μM, 72 h). (D) Quantitative graphs of these proteins levels. The results are presented as the mean ± SEM of at least three independent experiments and analyzed using one-way ANOVA followed by Bonferroni's post hoc test. *P<0.05, **P<0.01 and ***P<0.001.

NCT-58 simultaneously targets pro-survival HSP90 client proteins in TNBC cells. It was observed that NCT-58 significantly downregulated the expression of AKT and MEK and reduced their phosphorylation in MDA-MB-231 and 4T1 cells (P<0.05; Fig. 2A and B; Fig. S3A-F), suggesting that the simultaneous inhibition of these two major survival pathways could enhance the antiproliferative effect against TNBC cells.

STAT3 is activated by phosphorylation of its tyrosine residue (Tyr705) in response to stimulation by cytokines and growth factor receptors, and then translocates to the nucleus to promote the expression of survival factors such as cyclin D1, survivin, Bcl-2 and Bcl-xL (24). Therefore, inhibition of HSP90 may suppress the expression of several oncoproteins promoted by STAT3. It was observed that NCT-58 significantly impaired the expression and phosphorylation at Tyr705 of STAT3 in MDA-MB-231 and 4T1 cells, accompanied by the downregulation of survivin and cyclin D1 (P<0.01; Fig. 2C and D).

NCT-58 hampers cancer stem-like characteristics and migratory ability in TNBC cells. BCSCs confer resistance to chemotherapy during TNBC treatment and are thought to be a prerequisite for invasion and metastasis (8). It was examined whether NCT-58 affects BCSC-like properties, ALDH1 activity, $CD44^{high}/CD24^{low}$ stem-like populations, and mammosphere formation. Treatment with NCT-58 significantly suppressed ALDH1 activity in MDA-MB-231 (P<0.01; Fig. 3A) and 4T1 cells (P<0.01; Fig. 3B). The $CD44^{high}/CD24^{low}$ phenotype is associated with a higher incidence of relapse or distant metastasis (25). A significant reduction in the $CD44^{high}/CD24^{low}$-population was observed in MDA-MB-231 cells after NCT-58 challenge (P<0.001; Fig. 3C). Mammosphere 3D culture is a useful tool for assessing the tumor-like properties of BCSCs capable of propagating mammary and progenitor cells *in vitro* (26,27). The assay revealed that NCT-58 attenuated the mammosphere-forming ability, as evidenced by significant reductions in the number and volume of mammospheres derived from 4T1 cells (P<0.001; Fig. 3D).

Actin and vimentin are major HSP90 target proteins and cytoskeletal components that play important roles in cell interaction, motility, invasiveness and adhesion (13,28). Vimentin intermediate filament is a hallmark of EMT, and appears to be involved in TNBC metastasis (29). To explore whether NCT-58 affected the expression of HSP90 target cytoskeletons, the spatial distribution of vimentin and filamentous-actin was observed using immunofluorescence analysis. NCT-58 treatment resulted in vimentin and F-actin reorganization and the disruption of filament networks, resulting in concomitant cytoplasmic contraction and cellular rounding (Fig. 3E and F). Kinetic analysis of cell migration revealed that NCT-58 significantly and dose-dependently reduced the migration of both MDA-MB-231 and 4T1 cells *in vitro* (P<0.05; Fig. 3G and H), indicating that the collapse

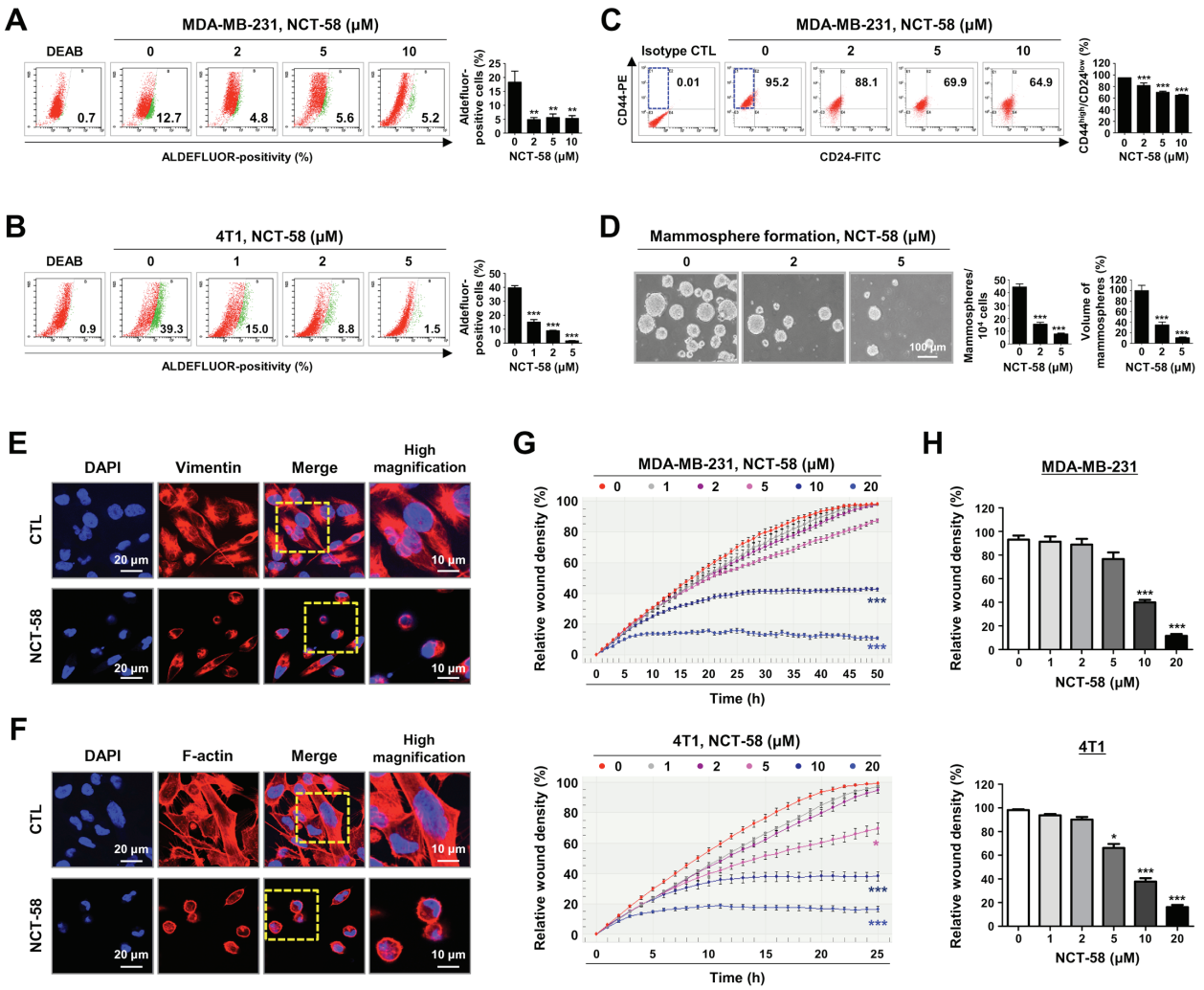

Figure 3. NCT-58 suppresses cancer stem-like properties and migratory activity in TNBC cells. (A and B) Effect of NCT-58 (0-10 μM, 72 h) on ALDH1 activity in (A) MDA-MB-231 and (B) 4T1 cells. The specific inhibitor diethyl-amino-benzaldehyde was used to define the Aldefluor-positive population. Aldefluor-positive cells were quantified using flow cytometry (right panel). (C) Effect of NCT-58 (0-10 μM, 72 h) on the $CD44^{high}/CD24^{low}$ stem-like population in MDA-MB-231 cells. The $CD44^{high}/CD24^{low}$ population was quantified through flow cytometry. (D) Effect of NCT-58 on mammosphere formation *in vitro*. 4T1 cells ($5x10^4$ cells/ml) were cultured in ultralow attachment plates in the presence or absence of NCT-58 (2-5 μM, 5 days). The number and volume of mammospheres were quantified using optical microscopy. (E and F) After exposure to NCT-58 (10 μM) for 48 h, MDA-MB-231 cells were immuno-stained for vimentin (1:100, E) and F-actin (1:100, Texas Red-X phalloidin, F) with DAPI nuclear stain (blue). (G and H) Effect of NCT-58 on TNBC cell migration. (G) After exposure to NCT-58 (0-20 μM) in MDA-MB-231 and 4T1 cells, kinetic analysis of cell migration was determined using the IncuCyte™ Live-Cell Imaging System and quantified for the indicated time duration. The kinetic graphs of cell migration represent the relative wound density. (H) Relative wound density (%) in MDA-MB-231 cells at 50 h and in 4T1 cells at 25 h, respectively. The results are presented as the mean ± SEM of at least three independent experiments and analyzed using one- or two-way ANOVA followed by Bonferroni's post hoc test. $^{*}P<0.05$, $^{**}P<0.01$ and $^{***}P<0.001$. TNBC, triple-negative breast cancer.

of filament dynamics may contribute to the suppression of migratory ability.

NCT-58 significantly enhances the anti-proliferative effects of paclitaxel and doxorubicin in a synergistic manner. It was investigated whether NCT-58 could enhance the sensitivity of cells to the conventional chemotherapeutic agents paclitaxel and doxorubicin. To assess the synergistic effects of NCT-58 on paclitaxel- or doxorubicin-induced suppression of cell viability, MDA-MB-231 cells were treated with NCT-58 (0-20 μM) combined with paclitaxel (0-2 μM) or doxorubicin (0-3 μM) for 72 h. The interaction between NCT-58 and paclitaxel or doxorubicin was evaluated by isobologram analysis, which uses a graphical representation (isobole) to assess drug effects. Additive interactions are represented as points along the line connecting the effective concentration 50 (EC_{50}) values of each drug, whereas the co-treatment of NCT-58 with paclitaxel or doxorubicin demonstrated synergistic effects, as indicated by points positioned below the isobole (Fig. 4A and D). The heat map intensity represents the relative cell viability of drug combination effects compared with the control treatment with DMSO alone (Fig. 4B and E). The CI further confirmed these synergistic interactions, highlighting the potential of NCT-58 to enhance the efficacy of conventional cytotoxic agents (Fig. 4C and F).

Discussion

In the present study, it was demonstrated that NCT-58, a C-terminal HSP90 inhibitor, exerts multifaceted antitumor effects in TNBC. Classical HSP90 inhibitors have not been successful owing to concerns regarding off-target toxicity

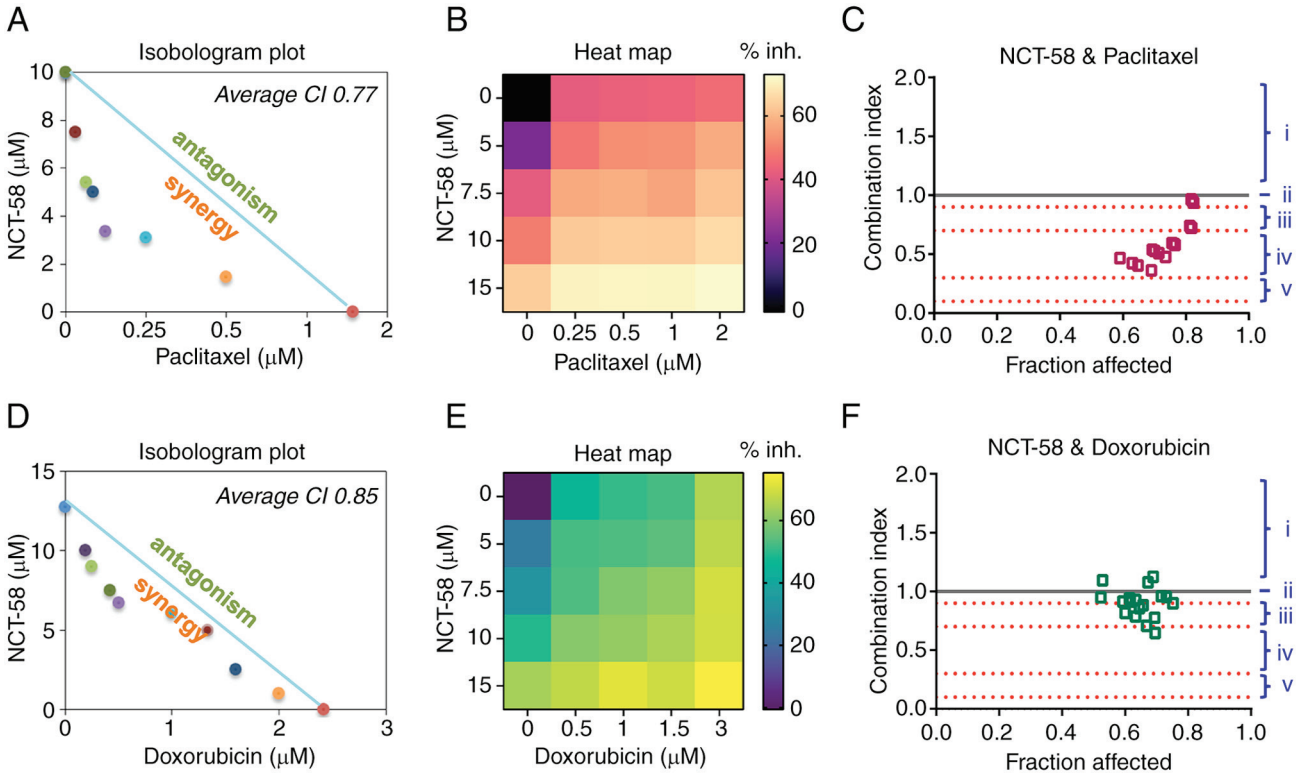

Figure 4. Synergistic effects of combining NCT-58 with paclitaxel or doxorubicin in triple-negative breast cancer cells. (A-F) MDA-MB-231 cells were treated with the indicated concentrations of NCT-58 (0-15 μM) and paclitaxel (0-2 μM, A-C) or doxorubicin (0-3 μM, D-F) for 72 h and cell viability was assessed using MTS assay. The isobologram plot, heat map (% inh., Inhibition rate), and CI were analyzed to assess the drug-drug synergy of various dose combinations of NCT-58 with paclitaxel or doxorubicin. Isobologram plot and average CI values were generated using the CompuSyn software to quantify drug interactions, where CI<1 indicates synergism, CI=1 indicates an additive effect, and CI>1 indicates antagonism. (i, antagonism; ii, addictive effect; iii, moderate synergism; iv, synergism; and v, strong synergism). The heat map depicts relative cell viability compared with the DMSO control. CI, combination index.

and the induction of HSR, which leads to cytoprotective responses (14,15). N-terminal HSP90 inhibitors trigger HSF-1 activation and translocation into the nucleus, resulting in elevated transcription of HSPs such as HSP70 and HSP90, which promote pro-survival signaling (15,22). NCT-58 effectively suppressed cell viability and induced apoptosis without triggering the HSR, which is a major limitation of current HSP90 inhibitors. Although geldanamycin, a N-terminal HSP90 inhibitor, markedly induced HSF-1 nuclear translocation and the subsequent upregulation of HSP70, NCT-58 did not produce these effects. This finding suggests that inhibiting the CTD prevents a key pitfall of numerous existing HSP90 inhibitors, namely the cytoprotective feedback loop, which diminishes therapeutic efficacy and enhances cytotoxicity in normal cells. The present data revealed the minimal cytotoxic effects of NCT-58 in normal mammary epithelial (MCF10A) and 293 cells, whereas geldanamycin significantly suppressed cell viability at considerably lower concentrations.

Mechanistically, NCT-58 simultaneously disrupted the functions of multiple HSP90 client proteins. By blocking HSP90 C-terminal dimerization, NCT-58 caused pronounced downregulation of AKT, MEK and STAT3, which are the major pro-survival pathways in TNBC. Previous genomic profiling revealed STAT3 overexpression and aberrant activation in TNBC, highlighting its potential as both a molecular target and biomarker (24,30). STAT3 inhibition is associated with reduced transcription of critical survival genes such as survivin and cyclin D1. Consistent with this observation, NCT-58 treatment decreased STAT3 activation and its downstream targets, thereby enhancing apoptosis and diminishing proliferative capacity. A particularly notable finding was the ability of NCT-58 to target the CSC-like properties of TNBC cells. The CSC subpopulation, typically characterized by elevated ALDH1 activity and a $CD44^{high}/CD24^{low}$ phenotype, plays a pivotal role in tumor initiation and recurrence (27,31). These cells exhibit robust self-renewal abilities and multipotency, which contribute to their resistance to conventional chemotherapy and radiotherapy (32). ALDH is a detoxifying enzyme and its ability to convert retinol to retinoic acid is implicated in cancer cell proliferation and CSC differentiation (33). Cyclophosphamide, a commonly used chemotherapy agent for TNBC, undergoes inactivation through ALDH-mediated oxidation during its metabolic process (34,35). Consequently, patients with elevated ALDH expression often experience relatively poor clinical outcomes and exhibit resistance to alkylating agents such as cyclophosphamide and ifosfamide (31,35,36). Therefore, strategies targeting ALDH activity show significant promise for the effective eradication of CSCs and the prevention of chemoresistance and recurrence. Treatment with NCT-58 significantly reduced ALDH1 activity and decreased the percentage of $CD44^{high}/CD24^{low}$ cells, ultimately impairing mammosphere formation in 3D culture. These data align with those of previous reports implicating HSP90 in the maintenance of CSC phenotypes and highlight the importance of targeting CSCs to minimize relapse and

metastasis. Accordingly, the 4T1 cell line was employed, which exhibits highly aggressive and stem cell-like characteristics, and is widely recognized as a preclinical model for evaluating cancer stemness and metastatic potential (37-39). In the *in vitro* experiments of the present study, 4T1 cells clearly demonstrated that NCT-58 reduces CSC-related traits such as ALDH1 activity, thereby supporting the results observed in human MDA-MB-231 cells. By simultaneously affecting both bulk tumor cells and CSC-like populations, NCT-58 can potentially overcome the major mechanisms of resistance in TNBC.

NCT-58 also inhibited cell migration, likely by modulating the HSP90 client proteins, vimentin and F-actin. During EMT, vimentin orchestrates cytoskeletal organization and cell-matrix interactions, enabling cancer cells to remodel the extracellular matrix and adopt a more flexible and invasive phenotype (40). Consequently, vimentin-enriched cells are more elastic and motile, facilitating tissue invasion, vascular or lymphatic entry, and survival under mechanical stress (41,42). By disrupting vimentin and F-actin filament dynamics, NCT-58 induced cytoskeletal reorganization and collapse, thereby reducing the migratory capacity of TNBC cells.

In a previous investigation by the authors, it was demonstrated that NCT-58 overcomes trastuzumab resistance in HER2-positive breast cancer by destabilizing HER2 family proteins, including HER2, HER3, Akt and truncated p95HER2. Moreover, NCT-58 downregulated the RAS/RAF/MEK/ERK pathway, thereby impairing downstream oncogenic signaling (16). These findings established NCT-58 as a promising therapeutic option for trastuzumab-resistant HER2-positive disease. In the present study, these observations were extended to TNBC, and it was shown that NCT-58 suppresses multiple HSP90 client proteins such as AKT, MEK and STAT3, leading to impaired pro-survival signaling, reduced cancer stem-like traits, and diminished migratory potential. Notably, distinct HSP90 client proteins are expressed depending on the breast cancer subtype (43,44). By targeting HSP90, NCT-58 can modulate these subtype-specific proteins and thereby block the oncogenic pathways that drive tumor growth in a subtype-specific manner. Collectively, the results of the present study highlight NCT-58 as a versatile therapeutic strategy with efficacy across different breast cancer subtypes.

Conventional treatments for TNBC are typically dependent on anthracyclines and taxanes. In recent years, immunotherapies and antibody-drug conjugates have broadened therapeutic options, prompting the latest National Comprehensive Cancer Network guidelines to recommend combining pembrolizumab with chemotherapy in PD-L1-positive cases (combined positive score ≥10). Sacituzumab-govitecan (SC) is an additional treatment option for advanced TNBC following first-line treatment failure (45). However, these approaches are limited by stringent biomarker requirements, suboptimal patient eligibility rates (~40% only qualify for immunotherapy) (46), and the potential for acquired resistance or cost-ineffectiveness (47). For instance, TNBC cells exposed to SC can eventually develop resistance by altering both the antibody target and toxic payload (48). Consequently, achieving sustained therapeutic efficacy in TNBC remains a significant clinical challenge.

Combination regimens are often required to address the heterogeneity of TNBC and forestall the emergence of drug resistance. NCT-58 exhibited synergistic anti-proliferative effects when co-administered with paclitaxel or doxorubicin, two foundational chemotherapeutic agents frequently used in TNBC. CI analysis confirmed this synergy, suggesting that the simultaneous disruption of HSP90 client protein function by NCT-58 may sensitize TNBC cells to cytotoxic agents.

Overall, the findings of the present study suggested that NCT-58 is a promising therapeutic candidate for TNBC, targeting both proliferative tumor cells and cancer stem-like populations, while avoiding the limitations of classical HSP90 inhibitors. By targeting key oncogenic pathways, including AKT, MEK and STAT3, NCT-58 significantly compromises cancer cell survival and induces apoptosis. Notably, NCT-58 exhibited minimal cytotoxicity in non-malignant cells, highlighting its favorable therapeutic profile. The present study has certain limitations, as additional *in vivo* validation is warranted. In particular, investigations using a 4T1-derived syngeneic model will be necessary to further elucidate the effects of NCT-58 on tumor growth, angiogenesis, metastasis, and the tumor microenvironment. Furthermore, comprehensive preclinical studies evaluating long-term toxicity and safety will be essential prior to clinical application in TNBC patients. Finally, NCT-58 enhances the anticancer efficacy of standard chemotherapeutic agents such as paclitaxel and doxorubicin in a synergistic manner, highlighting its potential as a potent and well-tolerated treatment option for TNBC.

Acknowledgements

Not applicable.

Funding

The present study was supported by the Korea Health Technology R&D Project through the Korea Health Industry Development Institute, funded by the Ministry of Health and Welfare, Republic of Korea (grant nos. HA17C0053 and HR20C0021); the National Research Foundation funded by the Korean government (grant nos. 2021R1A2C2009723, 2023R1A2C3004010,RS-2024-00342677,RS-2025-02634306 and RS-2025-00558356); the Korea University Guro Hospital (grant no. O2411391) and the Brain Korea 21 Plus Program.

Availability of data and materials

The data generated in the present study are included in the figures and/or tables of this article.

Authors' contributions

EJ, KL, JL, YJK, JYK and JHS conceived and designed the experiments. SJ, EJ, SP, KL, EO, DK, YJK and JYK performed the experiments. EJ, SJ, KL, SP, MP, DK, SK, YKK, KDN, YJK, LF and JYK analyzed the data. CTN, MTL, and JA synthesized NCT-58. EJ, KL, LF, YJK and JYK wrote the manuscript. EJ, JYK and YJK confirm the authenticity of all the raw data. All authors read and approved the final version of the manuscript.

Ethics approval and consent to participate

Not applicable.

Patient consent for publication

Not applicable.

Competing interests

The authors declare that they have no competing interests.

References

1. Zagami P and Carey LA: Triple negative breast cancer: Pitfalls and progress. NPJ Breast Cancer 8: 95, 2022.
2. Ferrarini M, Heltai S, Zocchi MR and Rugarli C: Unusual expression and localization of heat-shock proteins in human tumor cells. Int J Cancer 51: 613-619, 1992.
3. Pick E, Kluger Y, Giltnane JM, Moeder C, Camp RL, Rimm DL and Kluger HM: High HSP90 expression is associated with decreased survival in breast cancer. Cancer Res 67: 2932-2937, 2007.
4. Isaacs JS, Xu W and Neckers L: Heat shock protein 90 as a molecular target for cancer therapeutics. Cancer Cell 3: 213-217, 2003.
5. Bocchini CE, Kasembeli MM, Roh SH and Tweardy DJ: Contribution of chaperones to STAT pathway signaling. JAKSTAT 3: e970459, 2014.
6. Streicher JM: The role of heat shock proteins in regulating receptor signal transduction. Mol Pharmacol 95: 468-474, 2019.
7. Edkins AL: Hsp90 co-chaperones as drug targets in cancer: Current perspectives. In: Heat Shock Protein Inhibitors. McAlpine S and Edkins A (eds). Topics in Medicinal Chemistry. Vol 19. Springer, Cham, pp21-54, 2016.
8. Collina F, Di Bonito M, Li Bergolis V, De Laurentiis M, Vitagliano C, Cerrone M, Nuzzo F, Cantile M and Botti G: Prognostic value of cancer stem cells markers in triple-negative breast cancer. Biomed Res Int 2015: 158682, 2015.
9. Kabakov A, Yakimova A and Matchuk O: Molecular chaperones in cancer stem cells: Determinants of stemness and potential targets for antitumor therapy. Cells 9: 892, 2020.
10. Cho TM, Kim JY, Kim YJ, Sung D, Oh E, Jang S, Farrand L, Hoang VH, Nguyen CT, Ann J, *et al*: C-terminal HSP90 inhibitor L80 elicits anti-metastatic effects in triple-negative breast cancer via STAT3 inhibition. Cancer Lett 447: 141-153, 2019.
11. Park JM, Kim YJ, Park S, Park M, Farrand L, Nguyen CT, Ann J, Nam G, Park HJ, Lee J, *et al*: A novel HSP90 inhibitor targeting the C-terminal domain attenuates trastuzumab resistance in HER2-positive breast cancer. Mol Cancer 19: 161, 2020.
12. Park M, Jung E, Park JM, Park S, Ko D, Seo J, Kim S, Nam KD, Kang YK, Farrand L, *et al*: The HSP90 inhibitor HVH-2930 exhibits potent efficacy against trastuzumab-resistant HER2-positive breast cancer. Theranostics 14: 2442-2463, 2024.
13. Hoter A, El-Sabban ME and Naim HY: The HSP90 family: Structure, regulation, function, and implications in health and disease. Int J Mol Sci 19: 2560, 2018.
14. Garcia-Carbonero R, Carnero A and Paz-Ares L: Inhibition of HSP90 molecular chaperones: Moving into the clinic. Lancet Oncol 14: e358-e369, 2013.
15. Wang Y and McAlpine SR: N-terminal and C-terminal modulation of Hsp90 produce dissimilar phenotypes. Chem Commun (Camb) 51: 1410-1413, 2015.
16. Park S, Kim YJ, Park JM, Park M, Nam KD, Farrand L, Nguyen CT, La MT, Ann J, Lee J, *et al*: The C-terminal HSP90 inhibitor NCT-58 kills trastuzumab-resistant breast cancer stem-like cells. Cell Death Discov 7: 354, 2021.
17. Nguyen CT, Ann J, Sahu R, Byun WS, Lee S, Nam G, Park HJ, Park S, Kim YJ, Kim JY, *et al*: Discovery of novel anti-breast cancer agents derived from deguelin as inhibitors of heat shock protein 90 (HSP90). Bioorg Med Chem Lett 30: 127374, 2020.
18. Kim JY, Cho TM, Park JM, Park S, Park M, Nam KD, Ko D, Seo J, Kim S, Jung E, *et al*: A novel HSP90 inhibitor SL-145 suppresses metastatic triple-negative breast cancer without triggering the heat shock response. Oncogene 41: 3289-3297, 2022.
19. Donnelly A and Blagg BSJ: Novobiocin and additional inhibitors of the Hsp90 C-terminal nucleotide-binding pocket. Curr Med Chem 15: 2702-2717, 2008.
20. Stebbins CE, Russo AA, Schneider C, Rosen N, Hartl FU and Pavletich NP: Crystal structure of an Hsp90-geldanamycin complex: Targeting of a protein chaperone by an antitumor agent. Cell 89: 239-250, 1997.
21. Gooljarsingh LT, Fernandes C, Yan K, Zhang H, Grooms M, Johanson K, Sinnamon RH, Kirkpatrick RB, Kerrigan J, Lewis T, *et al*: A biochemical rationale for the anticancer effects of Hsp90 inhibitors: Slow, tight binding inhibition by geldanamycin and its analogues. Proc Natl Acad Sci USA 103: 7625-7630, 2006.
22. Wu J, Liu T, Rios Z, Mei Q, Lin X and Cao S: Heat shock proteins and cancer. Trends Pharmacol Sci 38: 226-256, 2017.
23. Neckers L, Blagg B, Haystead T, Trepel JB, Whitesell L and Picard D: Methods to validate Hsp90 inhibitor specificity, to identify off-target effects, and to rethink approaches for further clinical development. Cell Stress Chaperones 23: 467-482, 2018.
24. Qin JJ, Yan L, Zhang J and Zhang WD: STAT3 as a potential therapeutic target in triple negative breast cancer: A systematic review. J Exp Clin Cancer Res 38: 195, 2019.
25. Wang H, Wang L, Song Y, Wang S, Huang X, Xuan Q, Kang X and Zhang Q: $CD44^+/CD24^-$ phenotype predicts a poor prognosis in triple-negative breast cancer. Oncol Lett 14: 5890-5898, 2017.
26. Mani SA, Guo W, Liao MJ, Eaton EN, Ayyanan A, Zhou AY, Brooks M, Reinhard F, Zhang CC, Shipitsin M, *et al*: The epithelial-mesenchymal transition generates cells with properties of stem cells. Cell 133: 704-715, 2008.
27. Oh E, Kim YJ, An H, Sung D, Cho TM, Farrand L, Jang S, Seo JH and Kim JY: Flubendazole elicits anti-metastatic effects in triple-negative breast cancer via STAT3 inhibition. Int J Cancer 143: 1978-1993, 2018.
28. Zhang MH, Lee JS, Kim HJ, Jin DI, Kim JI, Lee KJ and Seo JS: HSP90 protects apoptotic cleavage of vimentin in geldanamycin-induced apoptosis. Mol Cell Biochem 281: 111-121, 2006.
29. Yamashita N, Tokunaga E, Kitao H, Hisamatsu Y, Taketani K, Akiyoshi S, Okada S, Aishima S, Morita M and Maehara Y: Vimentin as a poor prognostic factor for triple-negative breast cancer. J Cancer Res Clin Oncol 139: 739-746, 2013.
30. Sirkisoon SR, Carpenter RL, Rimkus T, Anderson A, Harrison A, Lange AM, Jin G, Watabe K and Lo HW: Interaction between STAT3 and GLI1/tGLI1 oncogenic transcription factors promotes the aggressiveness of triple-negative breast cancers and HER2-enriched breast cancer. Oncogene 37: 2502-2514, 2018.
31. Ginestier C, Hur MH, Charafe-Jauffret E, Monville F, Dutcher J, Brown M, Jacquemier J, Viens P, Kleer CG, Liu S, *et al*: ALDH1 is a marker of normal and malignant human mammary stem cells and a predictor of poor clinical outcome. Cell Stem Cell 1: 555-567, 2007.
32. Wei Y, Li Y, Chen Y, Liu P, Huang S, Zhang Y, Sun Y, Wu Z, Hu M, Wu Q, *et al*: ALDH1: A potential therapeutic target for cancer stem cells in solid tumors. Front Oncol 12: 1026278, 2022.
33. Clark DW and Palle K: Aldehyde dehydrogenases in cancer stem cells: Potential as therapeutic targets. Ann Transl Med 4: 518, 2016.
34. Sládek NE: Aldehyde dehydrogenase-mediated cellular relative insensitivity to the oxazaphosphorines. Curr Pharm Des 5: 607-625, 1999.
35. Sladek NE: Metabolism of oxazaphosphorines. Pharmacol Ther 37: 301-355, 1988.
36. Moreb JS: Aldehyde dehydrogenase as a marker for stem cells. Curr Stem Cell Res Ther 3: 237-246, 2008.
37. Schrörs B, Boegel S, Albrecht C, Bukur T, Bukur V, Holtsträter C, Ritzel C, Manninen K, Tadmor AD, Vormehr M, *et al*: Multi-omics characterization of the 4T1 murine mammary gland tumor model. Front Oncol 10: 1195, 2020.
38. Herndon ME, Ayers M, Gibson-Corley KN, Wendt MK, Wallrath LL, Henry MD and Stipp CS: The highly metastatic 4T1 breast carcinoma model possesses features of a hybrid epithelial/mesenchymal phenotype. Dis Model Mech 17: dmm050771, 2024.
39. Tao K, Fang M, Alroy J and Sahagian GG: Imagable 4T1 model for the study of late stage breast cancer. BMC Cancer 8: 228, 2008.
40. Satelli A and Li S: Vimentin in cancer and its potential as a molecular target for cancer therapy. Cell Mol Life Sci 68: 3033-3046, 2011.
41. Thiery JP, Acloque H, Huang RYJ and Nieto MA: Epithelial-mesenchymal transitions in development and disease. Cell 139: 871-890, 2009.

42. Lu W and Kang Y: Epithelial-mesenchymal plasticity in cancer progression and metastasis. Dev Cell 49: 361-374, 2019.
43. Zagouri F, Bournakis E, Koutsoukos K and Papadimitriou CA: Heat shock protein 90 (hsp90) expression and breast cancer. Pharmaceuticals (Basel) 5: 1008-1020, 2012.
44. Wei H, Zhang Y, Jia Y, Chen X, Niu T, Chatterjee A, He P and Hou G: Heat shock protein 90: Biological functions, diseases, and therapeutic targets. MedComm (2020) 5: e470, 2024.
45. Gradishar WJ, Moran MS, Abraham J, Abramson V, Aft R, Agnese D, Allison KH, Anderson B, Burstein HJ, Chew H, *et al*: NCCN guidelines® insights: Breast cancer, version 4.2023. J Natl Compr Canc Netw 21: 594-608, 2023.
46. Cortes J, Rugo HS, Cescon DW, Im SA, Yusof MM, Gallardo C, Lipatov O, Barrios CH, Perez-Garcia J, Iwata H, *et al*: Pembrolizumab plus chemotherapy in advanced triple-negative breast cancer. N Engl J Med 387: 217-226, 2022.
47. Xie J, Li S, Li Y and Li J: Cost-effectiveness of sacituzumab govitecan versus chemotherapy in patients with relapsed or refractory metastatic triple-negative breast cancer. BMC Health Serv Res 23: 706, 2023.
48. Coates JT, Sun S, Leshchiner I, Thimmiah N, Martin EE, McLoughlin D, Danysh BP, Slowik K, Jacobs RA, Rhrissorrakrai K, *et al*: Parallel genomic alterations of antigen and payload targets mediate polyclonal acquired clinical resistance to sacituzumab govitecan in triple-negative breast cancer. Cancer Discov 11: 2436-2445, 2021.